



# CHORUS

This is the accepted manuscript made available via CHORUS. The article has been published as:

## Origin of the metal-insulator transition in ultrathin films of $\text{La}_{\{2/3\}}\text{Sr}_{\{1/3\}}\text{MnO}_{\{3\}}$

Zhaoliang Liao, Fengmiao Li, Peng Gao, Lin Li, Jiandong Guo, Xiaoqing Pan, R. Jin, E. W. Plummer, and Jiandi Zhang

Phys. Rev. B **92**, 125123 — Published 14 September 2015

DOI: [10.1103/PhysRevB.92.125123](https://doi.org/10.1103/PhysRevB.92.125123)

# The Origin of Metal-Insulator Transition in Ultrathin Films of $\text{La}_{2/3}\text{Sr}_{1/3}\text{MnO}_3$

Zhaoliang Liao<sup>1</sup>, Fengmiao Li<sup>2</sup>, Peng Gao<sup>3</sup>, Lin Li<sup>2</sup>, Jiandong Guo<sup>2</sup>, Xiaoqing Pan<sup>3</sup>, R. Jin<sup>1</sup>, E. W. Plummer<sup>1</sup> and Jiandi Zhang<sup>1\*</sup>

<sup>1</sup>*Dept. of Physics & Astronomy, Louisiana State University, Baton Rouge, LA 70803, USA*

<sup>2</sup>*Beijing National Laboratory for Condensed-Matter Physics and Institute of Physics, Chinese Academy of Sciences, Beijing 100190, China*

<sup>3</sup>*Department of Materials Science and Engineering, University of Michigan, Ann Arbor, MI 48109, USA*

## ABSTRACT

Many ultrathin films of transition-metal oxides exhibit nonmetallic behavior, in contrast to their metallic bulk counterpart, thus displaying a metal-insulator transition (MIT) as the film thickness is reduced. The nature of this MIT has been a long-standing issue in the epitaxial oxide research community. Here we report a study of the processing dependence of the critical thickness ( $t_c$ ) of MIT and the origin of the insulating phase in  $\text{La}_{2/3}\text{Sr}_{1/3}\text{MnO}_3$  (LSMO) films. A  $t_c$  of 3 unit cells is achieved by minimizing oxygen vacancies under optimal growth conditions, diminishing the epitaxial strain with a tunable buffer layer, and suppressing surface strain by film capping. The electrical transport measurements demonstrate that the nonmetallic behavior in LSMO thin films is an unavoidable result of localization initiated by inherent disorder but amplified by the reduction in dimensionality.

\*email: [jiandiz@lsu.edu](mailto:jiandiz@lsu.edu)

Tailoring complex oxides for new functionality by artificial growth with atomic precision is a forefront area of research in condensed matter physics [1]. By introducing surface [2], interface [3], strain [4] and reduced dimensionality [5,6], interesting physical properties emerge, which can be fundamentally different from those exhibited in their corresponding bulk forms. The interface between two insulating oxides, such as  $\text{LaAlO}_3/\text{SrTiO}_3$ , exhibits 2D electron gas [7] and superconductivity [8]. In contrast, many films of metallic oxides, such as  $\text{SrVO}_3$  [5],  $\text{LaNiO}_3$  [9,10],  $\text{SrRuO}_3$  [11] and  $\text{La}_{1-x}\text{Sr}_x\text{MnO}_3$  [12-18], become nonmetallic in the ground state below a critical thickness ( $t_c$ ), thus referred as “dead” layer behavior. In spite of extensive research, the nature of such a thickness-driven metal-insulator transition (MIT) remains mysterious. In addition to an intrinsic driving force for the transition, extrinsic factors, such as film crystallinity and oxygen stoichiometry, also play vital roles in the transition [10,19]. How to avoid or minimize extrinsic effects and gain insight into the nature of the transition is the goal of this work.

$\text{La}_{2/3}\text{Sr}_{1/3}\text{MnO}_3$  (LSMO) is an attractive material for both fundamental physics concepts and potential technological application because it is a spin-polarized and the most itinerant electron material with the highest Curie temperature ( $T_C \sim 369$  K) among manganites [20]. However, the spin-polarized and metallic (referred as half-metal) character disappears as the material is prepared in the thin film form. The (001) oriented LSMO thin films are found to become insulating below a critical thickness, which depends on substrates and growth conditions [12-18]. Interface electronic reconstruction [17,21], such as orbital ordering, has been proposed to explain such a thickness-induced MIT. For example, Tebano *et al.* [17] and Lepetit *et al.* [21] showed that the LSMO films grown on  $\text{SrTiO}_3$  (STO) (001) substrates exhibit  $d_{3z^2-r^2}$  orbital ordering at the interface, thus resulting in nonmetallic behavior in the ultra-thin films. However, Huijben *et al.* revealed that there is no formation of such  $d_{3z^2-r^2}$  orbital ordering even in ultrathin films down to 3 u.c. thick [16]. Inconsistent values for the critical thickness ( $t_c$ ), such as 4.0 nm [14],

3.0 nm [16] and 2.7 nm [17] on STO (001), have been reported by different groups. Such inconsistency indicates that there must be some extrinsic effects involving in, such as structure imperfection [19] and oxygen deficiency [22]. The reported values of  $t_c$  for doped oxide films like LSMO are also larger than the critical thickness of several undoped metallic oxide films such as  $\text{LaNiO}_3$ ,  $\text{SrVO}_3$  and  $\text{SrRuO}_3$  [5,9-11], suggesting that the chemical inhomogeneity or A-site disorder in LSMO may enhance carrier localization and result in a larger  $t_c$ .

In this letter, we report a systematic study of critical thickness  $t_c$  for the MIT of LSMO by minimizing oxygen vacancies and engineering strain and interface. The minimum  $t_c$  of 3.u.c. for the MIT transition is achieved for STO-sandwiched LSMO films by diminishing the substrate-induced strain and surface effects. Through the analysis of low-temperature ( $T$ ) electrical transport property and Density-Function Theory (DFT) calculations, we conclude that the existence of finite experimental minimum  $t_c$  can be attributed to the localization effect which is induced probably by oxygen vacancies and/or A-site cation disorder. As film thickness is reduced, the effect of individual vacancy as a defect enhances. Such unavoidable localization serves as the universal “driving force” for the MIT in many ultrathin oxide films.

Figure 1a illustrates the lattice structure of ultrathin LSMO films epitaxially grown on STO (001), a widely used  $\text{ABO}_3$  perovskite substrate. The LSMO films were grown by ultrahigh vacuum-pulsed laser deposition. A KrF excimer laser ( $\lambda = 248$  nm) at a repetition rate of 3 Hz and a laser fluence of  $\sim 1$  J/cm<sup>2</sup> was used. The  $\text{TiO}_2$ -terminated STO (001) substrates [23] were used. To obtain an oxygen stoichiometry film, a strongly oxidant background gas ( $\text{O}_2+2\text{wt}\%\text{O}_3$ ) was utilized. During the growth the substrates were maintained at 700 °C. With this condition, a universal layer-by-layer growth was achieved for different oxidant gas partial pressure ( $P_{\text{O}}$ ) ranging from  $10^{-6}$  Torr to 180 mTorr. The atomically flat LSMO surface and sharp interface between LSMO/STO were achieved as characterized in the images with both scanning tunneling microscopy (STM) and scanning transmission electron microscopy (JOEL 2100F-STEM) shown in Fig. 1b-c. There is no obvious structure defect in our STEM cross-section image (see Fig. 1c)

within the LSMO film and at the interface. The step height as shown in Fig. 1b is  $\sim 0.39$  nm which equals one unit cell thickness. This indicates that the surface layer is identical. A 2D flat surface is also indicated by the RHEED pattern in inset of Fig. 1b. The surface topography of all films was also characterized by the RHEED patterns indicating 2D surfaces.

The oxygen stoichiometry was optimized by investigating the effect of oxygen partial pressure ( $P_O$ ) on the electrical and magnetic properties, which were measured by Physics Properties Measurement System (PPMS) and Quantum Design Superconducting Quantum Interference Device (SQUID), respectively. The resistivity was measured by standard four probe method. Figure 2a shows the  $T$ -dependence of resistivity ( $\rho$ ) of LSMO films grown at  $P_O$  of 130 mTorr for different film thickness. For thick films,  $\rho(T)$  exhibits a MIT with increasing temperature, similar to that in the bulk. However, the transition temperature ( $T_{MIT}$ ), which is defined by the peak position at  $d\rho/dT$  curve, decreases dramatically with decreasing film thickness. When the LSMO film is equal to or less than 6 u.c., the ground state of films becomes insulating rather than metallic seen in the thick films and bulk. Thus the critical thickness  $t_c = 6$  u.c. is obtained for the films grown at  $P_O = 130$  mTorr.

The critical thickness apparently varies with oxygen partial pressure. Figure 2b summarizes the thickness-dependence of  $T_{MIT}$  of the films grown at different  $P_O$  (from 1  $\mu$ Torr to 180 mTorr). Thus  $t_c$  is defined as the onset of the  $T_{MIT}$  for a given  $P_O$ . Note that  $t_c$  decreases and the saturated  $T_{MIT}$  ( $T_{MIT}^S$ , which is defined as the saturated value with film thickness) increases with increasing  $P_O$  until  $P_O \geq 80$  mTorr, indicating strong dependence on oxygen composition. To identify the saturated  $P_O$  for minimizing oxygen deficiency, we plot  $t_c$  and  $T_{MIT}^S$  as a function of  $P_O$  in Fig. 2c, respectively. As  $P_O \geq 80$  mTorr which referred as the optimized pressure for the growth, the minimum value of  $t_c$  (6 u.c.) is achieved.

There is a crossover thickness range above  $t_c$  before the film fully develops into bulk-like

properties [24], even grown under the optimized oxygen partial pressure. As shown in Fig. 2d for the films grown at  $P_O = 130$  mTorr,  $T_{MIT}$ , Curie temperature ( $T_C$ ) (determined from magnetization measurements) and the electrical conductivity  $\sigma$  ( $\sigma = 1/\rho$ ) measured at 6 K, increase with increasing thickness and then saturate around 15 u.c. at the values almost equal to these of the bulk [24]. The existence of such a crossover thickness range (from  $t_c = 6$  u.c. to  $\sim 15$  u.c.) indicates a gradual evolution of the film toward the bulk. Because of the difference in chemical composition [25] and lattice structure [26], the physical properties near surface and the interface cannot be the same as the inside of the film. This will result in a difference in overall film property from the bulk, especially when film is not thick enough. In contrast to the sharp onsets of  $T_{MIT}$  and electrical conductivity,  $T_C$  shows a gradual change across  $t_c$ . As shown in Fig. 2d, the 4 and 5 u.c. LSMO films on STO (001) are nonmetallic but exhibit ferromagnetism with  $T_C$  of 170 K and 265 K, respectively. Such decoupled magnetism and transport behavior in ultrathin films may be related to the localization effects which are important and will be discussed later.

After optimizing  $P_O$ , we are able to further investigate the substrate-induced strain effect on  $t_c$ . We have grown LSMO films on the substrates with different lattice constants under constant  $P_O = 130$  mTorr. A layer-by-layer growth mode was observed for film growth on these substrates. Figure 3a presents the dependence of the critical thickness on the lattice mismatch of different substrates to the bulk of LSMO ( $a_{LSMO} = 3.88$  Å) under pseudo-cubic perovskite structure. It is obvious that any substrate-induced strain as quantified by the lattice mismatch ( $\epsilon = \frac{a_{sub} - a_{LSMO}}{a_{LSMO}} \times 100\%$ ), either compressive such as from LaAlO<sub>3</sub> (LAO) (001) or tensile one from DyScO<sub>3</sub> (DSO) (110), results in a significant increase of  $t_c$ . With the smallest lattice mismatch  $\epsilon = -0.5\%$  for the film on NdGaO<sub>3</sub> (NGO) (110),  $t_c$  decreases to 5 u.c.. Therefore, it is expected that the minimum  $t_c$  is achieved for a strain-free film.

The thickness and strain effects on magnetization were investigated in an attempt to determine

the origin of dead layer. The temperature dependent magnetization for different thickness of LSMO films on STO is shown in Fig. 3b. It is clear that the ferromagnetism is greatly suppressed with reducing thickness but still survives in ultrathin films (even below  $t_c$ ), consistent with previous report from Huijben et al [16]. Therefore, there is clearly decoupling between ferromagnetism and transport.  $T_C$  for 6 uc LSMO/STO is still as high as  $\sim 280$  K. The decoupling of metallicity with ferromagnetism [16] indicates that the electric dead layer is not magnetic in origin.

Substrate strain dramatically affects the magnetic property in ultrathin LSMO films. A relative thick 10 uc LSMO film on LAO shows a significant weaker magnetization than that on STO (see Fig. 3c). The strongly suppression in magnetization of LSMO/LAO is due to the large compressive strain induced by LAO substrate, which enhances antiferromagnetism in LSMO by suppressing the double-exchange interactions [16,17]. A compressed strain, which elongates  $\text{MnO}_6$  octahedron, promotes the  $e_g-d_{3z^2-r^2}$  occupancy thus favors C-type AFM ordering.

To achieve strain-free or the minimum strain condition on LSMO films, we use strained STO buffer layer grown on NGO (110) substrate before growing LSMO films. Realizing the sequence of the lattice constant of these three materials,  $a_{NGO} < a_{LSMO} < a_{STO}$ , we are able to tune a proper thickness of STO buffer layer so that the surface lattice constant of STO layer relaxes toward  $a_{LSMO}$  from  $a_{NGO}$  of the substrate. Figure 3d shows the resistivity of 5 u.c. LSMO film grown on different thickness of the STO buffer layers on NGO (110) substrate. While the 5 u.c. LSMO film on NGO (110) is insulating, the introduction of STO buffer layer induces an insulator to metal transition when the buffer layer is thicker than 5 u.c.. The transition temperature  $T_{MIT}$  increases with increasing the buffer layer thickness from 5 to 9 u.c., and then decreases above 9 u.c.. Such non-monotonic variation of  $T_{MIT}$  on LSMO film with STO buffer layer thickness can be understood by the change of lattice strain (or  $\varepsilon$ ). Though there is no data on the lattice constant in the strained STO buffer layer as a function of thickness, our data implies that the 9

u.c. STO buffer layer on NGO results in the best lattice match (i.e., close to zero lattice-mismatch) to LSMO films, thus able to convert the 5 u.c. LSMO film to a metallic ground state. The optimized  $T_{\text{MIT}}$  of the 5 u.c. LSMO film on 9 u.c. STO buffer layer reaches  $\sim 252$  K. Similar to that shown in Fig. 2b,  $T_{\text{MIT}}$  quickly drops to zero when thickness is reduced to 4 u.c., indicating  $t_c = 4$  u.c. in this case.

Strain leads to the enhancement of nonmetallic behavior of LSMO. The tensile strain causes the flattening of  $\text{MnO}_6$  octahedron and the  $e_g$ -electron prefers to occupy  $d_{x^2-y^2}$  orbital [16,17,27,28], thus driving the system to be in an A-type AFM insulating state. The compressed strain, on the other hand, elongates  $\text{MnO}_6$  octahedron resulting in  $d_{3z^2-r^2}$  orbital ordering that favors the C-type AFM insulating phase. Now a question is: what is the origin of the finite  $t_c$ , even for a strain-free LSMO film? In an attempt to answer question we have performed first-principles calculations to study the electronic structure of single monolayer LSMO on STO substrate by using density functional theory plus on-site Coulomb interaction (DFT+U) approach. The results are displayed in Fig. 4. The calculations were carried out using the “Vienna *ab initio* simulation package” (VASP) code [29]. We used the projector augmented-wave method [30] and the Perdew-Burke-Ernzerhof functional [31] with kinetic energy 400 eV. The Hubbard U’s acting on the Ti and Mn 3d states are  $U_{\text{Ti}} = 8.0$  eV and  $U_{\text{Mn}} = 2.0$  eV, respectively. DFT+U calculation reproduces the ferromagnetic and half-metal properties in bulk LSMO [24,32]. To model the LSMO/STO interface, we adopt the  $(3 \times 1)$  slab model as shown in Fig. 4a with inversion symmetry along the direction normal to the film surface (*i.e.* out-of-plane direction). Only atoms in the film are relaxed along the out-of-plane direction until the force is less than  $0.05$  eV/Å with the  $(2 \times 6 \times 1)$  Monkhorst-pack  $k$ -point mesh. We employ the  $(3 \times 7 \times 1)$  Monkhorst-pack  $k$ -point mesh and  $0.1$  eV Gaussian smearing to plot the density of states (DOS) shown in Fig. 4b-c. The orbital-resolved DOS of single unit cell LSMO on STO from the DFT+U calculation is shown in Fig. 4b-c, where there is a finite density of states at  $E_F$  and ferromagnetic ordering in single u.c.

LSMO layer, indicating that ferromagnetic metallic ground state is robust against the pure spatial confinement (thus no dead layer). Defects such as oxygen vacancies are not considered in the calculations, which could alter the electronic structure near  $E_F$  significantly in the ultrathin film case and explain the experimental observation.

We have further investigated the effect of surface strain on  $t_c$  by capping the LSMO films with crystalline STO overlayers. It is found that the STO sandwiched LSMO films exhibit a smaller  $t_c$ . With 2 u.c. STO capping layer, the values of  $t_c$  for all the LSMO films directly grown on STO, NGO and NGO substrate with STO buffer layer are reduced by one unit cell. Figure 5a shows that 4 u.c. LSMO film grown on 9 u.c. STO buffered NGO(110) is insulating in the ground state without capping, but metallic with 2 u.c. STO capping layer. We have grown different thickness of LSMO films: [(STO)<sub>2</sub>/(LSMO)<sub>n</sub>/(STO)<sub>9</sub>/NGO] ( $n = 2, 3, 4, 5$ ) using both capping and buffer layers, The films show metallic ground state when the LSMO thickness is larger than 3 u.c. ( $n > 3$ ), as shown in Fig. 5b, For 3 u.c. LSMO, a cross-over non-metal to metal transition can be observed at  $\sim 77$  K, following a re-entrance of insulating state during cooling down. When  $n = 2$ , the film exhibits insulating in the whole measurable temperature range. Therefore, a minimum  $t_c = 3$  u.c. is achieved by sandwiching LSMO between two STO layers on NGO substrate. The STO capping effect on  $t_c$ , which is independent on substrates, indicates that the surface also plays an important role in physical properties of films. We note that the critical thickness for both LSMO/NGO and LSMO/STO (2u.c.)/NGO are identical, i.e., 5 u.c., while they have quite different interface. Therefore, the nature of substrate and capping layer themselves don't have strong impact on the dead layer thickness. The most likely explanation is that the STO capping layer removes the strain present at a free surface [33].

The results discussed above indicate that  $t_c$  can be reduced by proper growth procedures and by removing interface/surface strain, but  $t_c$  does not go to zero. Coupling this observation with the fact the calculations indicate that all films should be metallic, the conclusion must be that either extrinsic factors in the experiment or many-body factors left out of the theory must be considered.

In fact, we will illustrate with Fig. 6 that both of these phenomena seem to be important. The unavoidable presence of oxygen vacancies and cation disorder leads to a dimensional dependence in the transport properties caused by localization. Figure 6 presents the resistance  $\rho$  versus  $\log(T)$  for three different film thicknesses for LSMO grown on STO(001) (Fig. 2a). The curve for 60 u.c. thickness in Fig. 6a shows a slight deviation from metallic behavior at temperatures below  $\sim 10$  K, which is also seen in the bulk [24]. The low temperature linear behavior of the resistivity as a function of  $\log(T)$  becomes more pronounced as the film becomes thinner as shown for 7 u.c. thicknesses in Fig. 6b. This linear behavior is a signature of weak localization [34, 35]. But as the film becomes thinner the resistivity at low temperature deviates from linear as shown in Fig. 6c for 6 u.c. film. The inset in Fig. 6b shows the dependence of the slope of  $\rho$  versus  $\log(T)$  as a function of film thickness showing a dramatic change for the films near  $t_c$ . This data indicates that what is being observed is the change in the effect of localization with dimensionality [36]. Apparently the signature of weak localization is present down to  $\sim 7$  u.c. thickness, with the 6 u.c. film showing very nonlinear behavior in the  $\rho$  vs.  $\log(T)$  plot. The resistivity for 5 u.c. or thinner film displays an exponentially thermally activated behavior as shown in the inset of Fig. 6c. The slope of this plot gives the thermal activation energy of  $\sim 20$  meV.

The film with critical thickness of 6 u.c. LSMO on STO(001) cannot be categorized as either thermal activated or weak localized system. Instead, its transport behaves like variable-range hopping (VRH) type [34,37]. The low- $T$  resistivity exhibits linear behavior when plotted as  $\ln(\rho)$  versus  $T^{-1/3}$  (Fig. 6d), consistent with the Mott's quasi-two-dimensional (2D) VRH picture with  $\rho = \rho_0 \exp(T_0 / T)^\alpha$ . Here the exponent  $\alpha = 1/3$  corresponds to a quasi-two dimensional system [37]. This implies that there is nonzero density of states (DOS) at the Fermi energy ( $E_F$ ) (i.e., zero energy gap) and the transport relies on hopping [37]. The trend of low- $T$  resistivity behavior from 7 to 5 u.c. LSMO films clearly indicates an evolution from weak localization to strong localization with reducing thickness, eventually ending with insulating dead layer.

The transition from weak to strong localization is characterized by Ioffe-Regel limit of resistivity [34] above which the system is turned into strong localization region. For a 2D system, the Ioffe-Regel limit is related to sheet resistance of  $R_{IR} \approx 25 \text{ K}\Omega/\square$  [9,34]. As shown in Fig. 6e, we can find metallic films with weak localization (Fig. 6a-b) when the resistivity of the LSMO films on STO(001) is below Ioffe-Regel limit, while above the Ioffe-Regel limit, the films are nonmetallic. Similar results are observed for the STO sandwiched LSMO films on NGO (110) (2u.c STO/LSMO<sub>n</sub>/9 u.c. STO/NGO) where a gradual weak to strong localization is observed when decreasing the thickness, as shown in Fig. 7a-b. The Ioffe-Regel limit separates the metallic films from insulating films (See Fig. 7a). For metallic films, such as STO sandwiched 4 u.c. film, weak localization is observed at low- $T$  (Fig. 7b). With reducing thickness, the 3 u.c. film becomes strongly localized and obeys the 2D VRH transport behavior (Inset panel II in Fig. 7b). Further reducing the thickness below critical thickness, thermal activation is observed in 2 u.c. LSMO (Inset panel I in Fig. 7b). Similar transport behavior is also observed for LSMO films with thickness near  $t_c$  on different substrates, thus indicating a kind of universal evolution in transport with film thickness. The question to be answered by theory is, can this be explained by a dimensionality associated with Anderson localization, or does the physics change as the film becomes thinner. An understanding of the dimensionality-dependent localization would have a widespread impact of interface physics.

In summary, the nature of the insulating behavior of LSMO films is systematically investigated. The epitaxial strain, oxygen vacancy, and the surface effect, are found to enhance the nonmetallic behavior of LSMO films and increase  $t_c$  for metal-insulator transition. By minimizing these effects, an ultimate minimum  $t_c = 3$  u.c. is achieved. However, transport measurement indicates that dimensionally-dependent localization effects prevent the thin films from exhibiting metallic behavior. These localization effects are induced by A-site disorder and/or oxygen vacancies which exist in these materials and amplified by the reduced dimensionality.

*Acknowledgments.* We thank Ziyang Meng for fruitful discussions. This work was supported by

U.S. DOE under Grant No. DOE DE-SC0002136. F.L and J.G are supported by NSFC grant No. 11225422.

## References

- [1] C. H. Ahn, A. Bhattacharya, M. Di Ventra, J. N. Eckstein, C. D. Frisbie, M. E. Gershenson, A. M. Goldman, I. H. Inoue, J. Mannhart, A. J. Millis, A. F. Morpurgo, D. Natelson, J. -M. Triscone, Electrostatic modification of novel materials, *Rev. Mod. Phys.* **78**, 1185 (2006).
- [2] R. G. Moore, J. D. Zhang, V. B. Nascimento, R. Jin, J. D. Guo, G. T. Wang, Z. Fang, D. Mandrus, E. W. Plummer, A surface-tailored purely electronic Mott metal-to-insulator transition, *Science* **318**, 615 (2007).
- [3] H. Y. Hwang, Y. Iwasa, M. Kawasaki, B. Keimer, N. Nagaosa, Y. Tokura, Emergent phenomena at oxide interfaces, *Nature Mater.* **11**, 103 (2012).
- [4] D. G. Schlom, L. -Q. Chen, C. -B. Eom, K. M. Rabe, S. K. Streiffer, J. -M. Triscone, Strain tuning of ferroelectric thin films, *Ann. Rev. Mater. Res.* **37**, 589 (2007).
- [5] K. Yoshimatsu, T. Okabe, H. Kumigashira, S. Okamoto, S. Aizaki, A. Fujimori, M. Oshima, Dimensional-crossover-driven metal-insulator transition in SrVO<sub>3</sub> ultrathin films, *Phys. Rev. Lett.* **104**, 147601 (2010).
- [6] A. V. Boris, Y. Matiks, E. Benckiser, A. Frano, P. Popovich, V. Hinkov, P. Wochner, M. Castro-Colin, E. Detemple, V. K. Malik, C. Bernhard, T. Prokscha, A. Suter, Z. Salman, E. Morenzoni, G. Cristiani, H. -U. Habermeier, B. Keimer, Dimensionality control of electronic phase transitions in nickel-oxide superlattices, *Science* **332**, 937 (2011).
- [7] A. Ohtomo, H. Y. Hwang, A high-mobility electron gas at the LaAlO<sub>3</sub>/SrTiO<sub>3</sub> heterointerface, *Nature* **427**, 423 (2004).
- [8] N. Reyren, S. Thiel, A. D. Caviglia, L. F. Kourkoutis, G. Hammerl, C. Richter, C. W. Schneider, T. Kopp, A. -S. Rüetschi, D. Jaccard, M. Gabay, D. A. Muller, J. -M. Triscone, J. Mannhart, Superconducting interfaces between insulating oxides, *Science* **317**, 1196 (2007).
- [9] R. Scherwitzl, S. Gariglio, M. Gabay, P. Zubko, M. Gibert, J. -M. Triscone, Metal-Insulator Transition in Ultrathin LaNiO<sub>3</sub> Films, *Phys. Rev. Lett.* **106**, 246403 (2011).
- [10] P. D. C. King, H. I. Wei, Y. F. Nie, M. Uchida, C. Adamo, S. Zhu, X. He, I. Božović, D. G.

- Schlom, K. M. Shen, Atomic-scale control of competing electronic phases in ultrathin LaNiO<sub>3</sub>, *Nat. Nanotech.* **9**, 443 (2014).
- [11] J. Xia, W. Siemons, G. Koster, M. R. Beasley, A. Kapitulnik, Critical thickness for itinerant ferromagnetism in ultrathin films of SrRuO<sub>3</sub>, *Phys. Rev. B* **79**, 140407R (2009).
- [12] J. Z. Sun, D. W. Abraham, R. A. Rao, C. B. Eom, Thickness-dependent magnetotransport in ultrathin manganite films, *Appl. Phys. Lett.* **74**, 3017 (1999).
- [13] R. P. Borges, W. Guichard, J. G. Lunney, J. M. D. Coey, F. Ott, Magnetic and electric “dead” layers in (La<sub>0.7</sub>Sr<sub>0.3</sub>)MnO<sub>3</sub> thin films, *J. Appl. Phys.* **89**, 3868 (2001).
- [14] M. Angeloni, G. Balestrino, N. G. Boggio, P. G. Medaglia, P. Orgiani, A. Tebano, Suppression of the metal-insulator transition temperature in thin La<sub>0.7</sub>Sr<sub>0.3</sub>MnO<sub>3</sub> films, *J. Appl. Phys.* **96**, 6387(2004).
- [15] A. Tebano, C. Aruta, P. G. Medaglia, F. Tozzi, G. Balestrino, A. A. Sidorenko, G. Allodi, R. De Renzi, G. Ghiringhelli, C. Dallera, L. Braicovich, N. B. Brookes, Strain-induced phase separation in La<sub>0.7</sub>Sr<sub>0.3</sub>MnO<sub>3</sub> thin films, *Phys. Rev. B* **74**, 245116 (2006).
- [16] M. Huijben, L. W. Martin, Y. -H. Chu, M. B. Holcomb, P. Yu, G. Rijnders, D. H. A. Blank, R. Ramesh, Critical thickness and orbital ordering in ultrathin La<sub>0.7</sub>Sr<sub>0.3</sub>MnO<sub>3</sub> films, *Phys. Rev. B* **78**, 094413 (2008).
- [17] A. Tebano, C. Aruta, S. Sanna, P. G. Medaglia, G. Balestrino, A. A. Sidorenko, R. De Renzi, G. Ghiringhelli, L. Braicovich, V. Bisogni, N. B. Brookes, Evidence of orbital reconstruction at interfaces in ultrathin La<sub>0.67</sub>Sr<sub>0.33</sub>MnO<sub>3</sub> films, *Phys. Rev. Lett.* **100**, 137401 (2008).
- [18] B. J. Kim, D. Y. Kwon, T. Yajima, C. Bell, Y. Hikita, B. G. Kim, H. Y. Hwang, Reentrant insulating state in ultrathin manganite films, *Appl. Phys. Lett.* **99**, 092513(2011).
- [19] L. Fitting Kourkoutis, J. H. Song, H. Y. Hwang, D. A. Mullera, Microscopic origins for stabilizing room-temperature ferromagnetism in ultrathin manganite layers, *Proc. Natl. Acad. Sci. U.S.A.* **107**, 11682 (2010)..

- [20] Y. Tokura, Y. Tomioka, Colossal magnetoresistive manganites, *J. Magn. Magn. Matter.* **200**, 1 (1999).
- [21] M. B. Lepetit, B. Mercey, C. Simon, Interface effects in perovskite thin films, *Phys. Rev. Lett.* **108**, 087202 (2012).
- [22] J. R. Sun, H. W. Yeung, H. K. Wong, T. Zhu, B. G. Shen, Effects of vacuum annealing on the transport property of  $\text{La}_{0.67}\text{Sr}_{0.33}\text{MnO}_{3-\delta}$  films, *Eur. Phys. J.* **35**, 481 (2003).
- [23] G. Koster, B. L. Kropman, G. Rijnders, D. H. A. Blank, H. Rogalla, Quasi-ideal strontium titanate crystal surfaces through formation of strontium hydroxide, *Appl. Phys. Lett.* **73**, 2920 (1998).
- [24] A. Urushibara, Y. Moritomo, T. Arima, A. Asamitsu, G. Kido, Y. Tokura, Insulator-metal transition and giant magnetoresistance in  $\text{La}_{1-x}\text{Sr}_x\text{MnO}_3$ , *Phys. Rev. B* **51**, 14103 (1995).
- [25] H. Dulli, P. A. Dowben, S. -H. Liou, E. W. Plummer, Surface segregation and restructuring of colossal-magnetoresistant manganese perovskites  $\text{La}_{0.65}\text{Sr}_{0.35}\text{MnO}_3$ , *Phys. Rev. B* **62**, R14629 (2000).
- [26] A. Vailionis, H. Boschker, Z. Liao, J. R. A. Smit, G. Rijnders, M. Huijben, G. Koster, Symmetry and lattice mismatch induced strain accommodation near and away from correlated perovskite interfaces, *Appl. Phys. Lett.* **105**, 131906 (2014).
- [27] Z. Fang, I. V. Solovyev, K. Terakura, Phase diagram of tetragonal manganites, *Phys. Rev. Lett.* **84**, 3169 (2000).
- [28] Y. Konishi, Z. Fang, M. Izumi, T. Manako, M. Kasai, H. Kuwahara, M. Kawasaki, K. Terakura, Y. Tokura, Orbital-state-mediated phase-control of manganites, *J. Phys. Soc. Jpn.* **68**, 3790 (1999).
- [29] G. Kresse and J. Furthmuller, *Phys. Rev. B* **54**, 11169 (1996); G. Kresse and J. Hafner, Ab initio molecular dynamics for liquid metals, *Phys. Rev. B* **47**, R558 (1993).
- [30] P. E. Blochl, Projector augmented-wave method, *Phys. Rev. B* **50**, 17953 (1994).
- [31] J.P. Perdew, K. Burke, and M. Ernzerhof, Generalized Gradient Approximation Made

Simple, Phys. Rev. Lett. **77**, 3865 (1996).

[32] J. -H. Park, E. Vescovo, H. -J. Kim, C. Kwon, R. Ramesh, T. Venkatesan, Direct evidence for a half-metallic ferromagnet, *Nature (London)* **392**, 794 (1998).

[33] D. Pesquera, G. Herranz, A. Barla, E. Pellegrin, F. Bondino, E. Magnano, F. Sánchez, J. Fontcuberta, Surface symmetry-breaking and strain effects on orbital occupancy in transition metal perovskite epitaxial films, *Nat. Commun.* **3**, 1189 (2012).

[34] P. A. Lee, T. V. Ramakrishnan, Disordered electronic systems, *Rev. Mod. Phys.* **57**, 287 (1987).

[35] V. Dobrosavljevic, N. Trivedi, and J.M. Valles Jr., edited, *Conductor Insulator Quantum Phase Transitions*, Oxford University Press, 2012, ISBN 9780199592593.

[36] S. Datta, *Electronic transport in mesoscopic systems*, Cambridge University Press, 1997.

[37] W. Brenig, G.H. Dohler, and H. Heyszenau, Hopping conductivity in highly anisotropic systems, *Philos. Mag.* **27**, 1093 (1973).

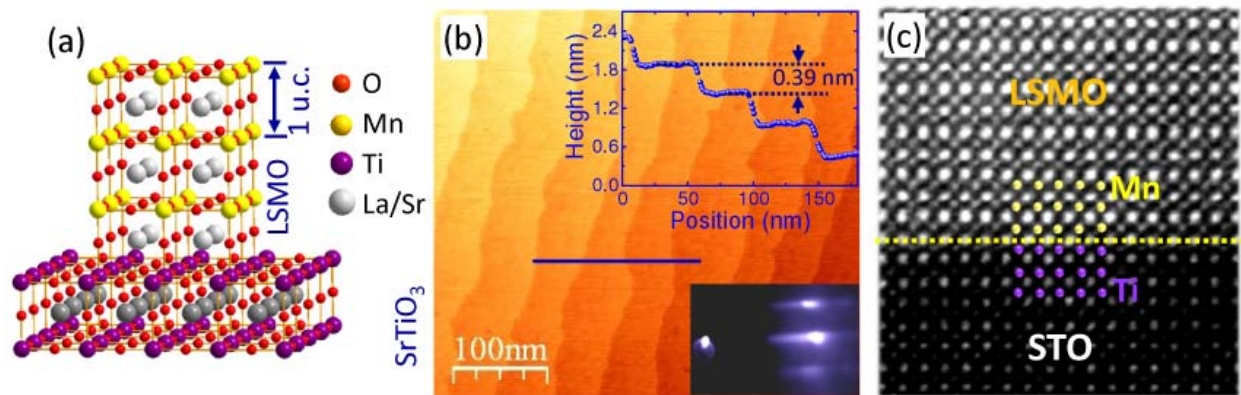


**Figure 1.** Atomically layer-by-layer growth of LSMO on STO (001): (a) Schematic structure model of a 3 unit cell LSMO on perovskite substrate. (b) Surface morphology of a 10 u.c. LSMO thin film on Nb-doped STO imaged by STM ( $V_{\text{tip}} = 2\text{V}$ ,  $I_t = 300\text{ pA}$ ). Inset shows the profile along the blue line. (c) Cross-section STEM image of the LSMO/STO. The film was grown at  $P_{\text{O}} = 80\text{ mTorr}$ .

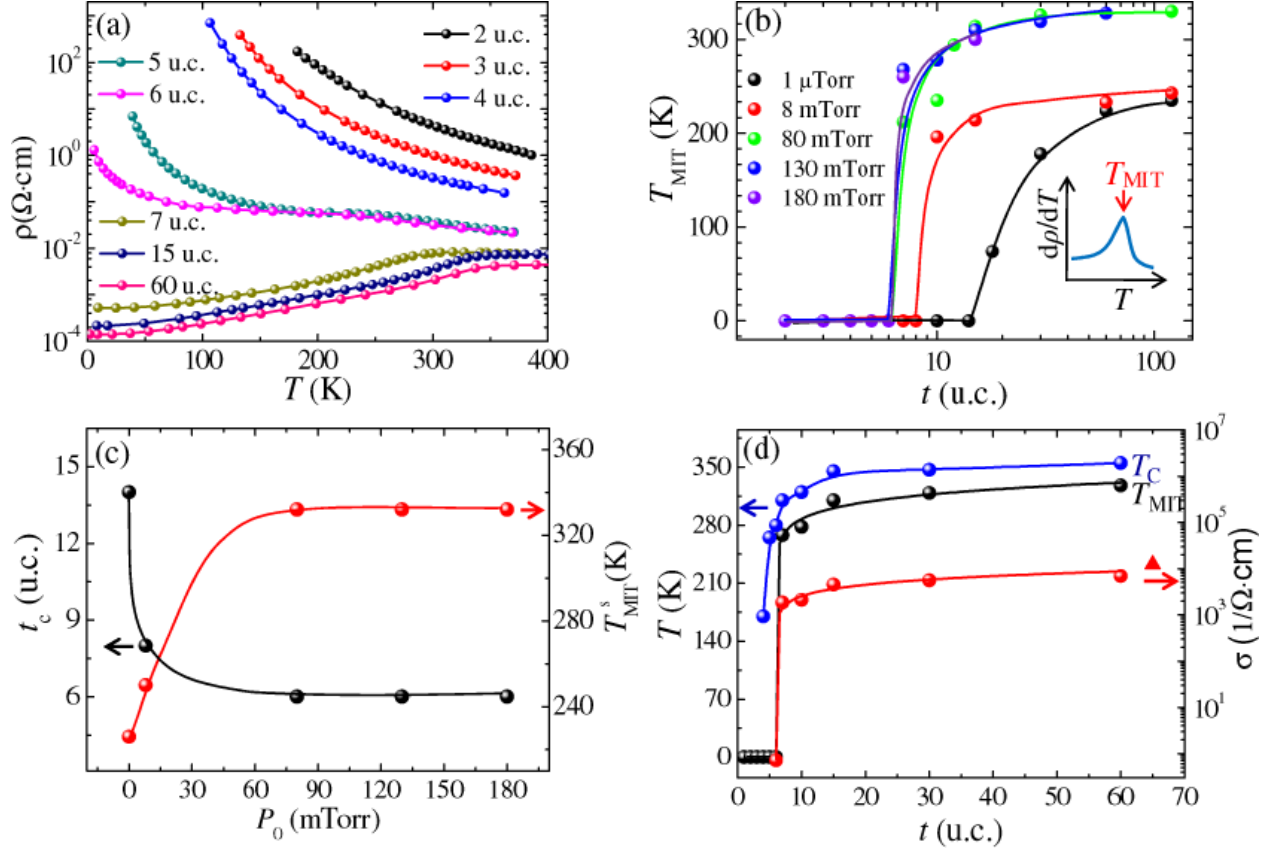


**Figure 2.** (a)  $T$ -dependence of resistivity of LSMO films grown on STO(001) at oxygen pressure  $P_O = 130$  mTorr for different thickness. (b) Thickness-dependence of  $T_{\text{MIT}}$  for the LSMO films grown at different  $P_O$ .  $T_{\text{MIT}}$  is determined by the maximum of the first derivative of resistivity versus temperature (see inset). (c)  $P_O$ -dependence of the critical thickness ( $t_c$ ) for MIT and the saturated  $T_{\text{MIT}}$  ( $T_{\text{MIT}}^S$ ) of LSMO films. (d) Thickness-dependence of Curie temperature  $T_C$  (blue),  $T_{\text{MIT}}$  (black), and conductivity  $\sigma$  at 6 K (red) of the LSMO films grown at  $P_O = 130$  mTorr.

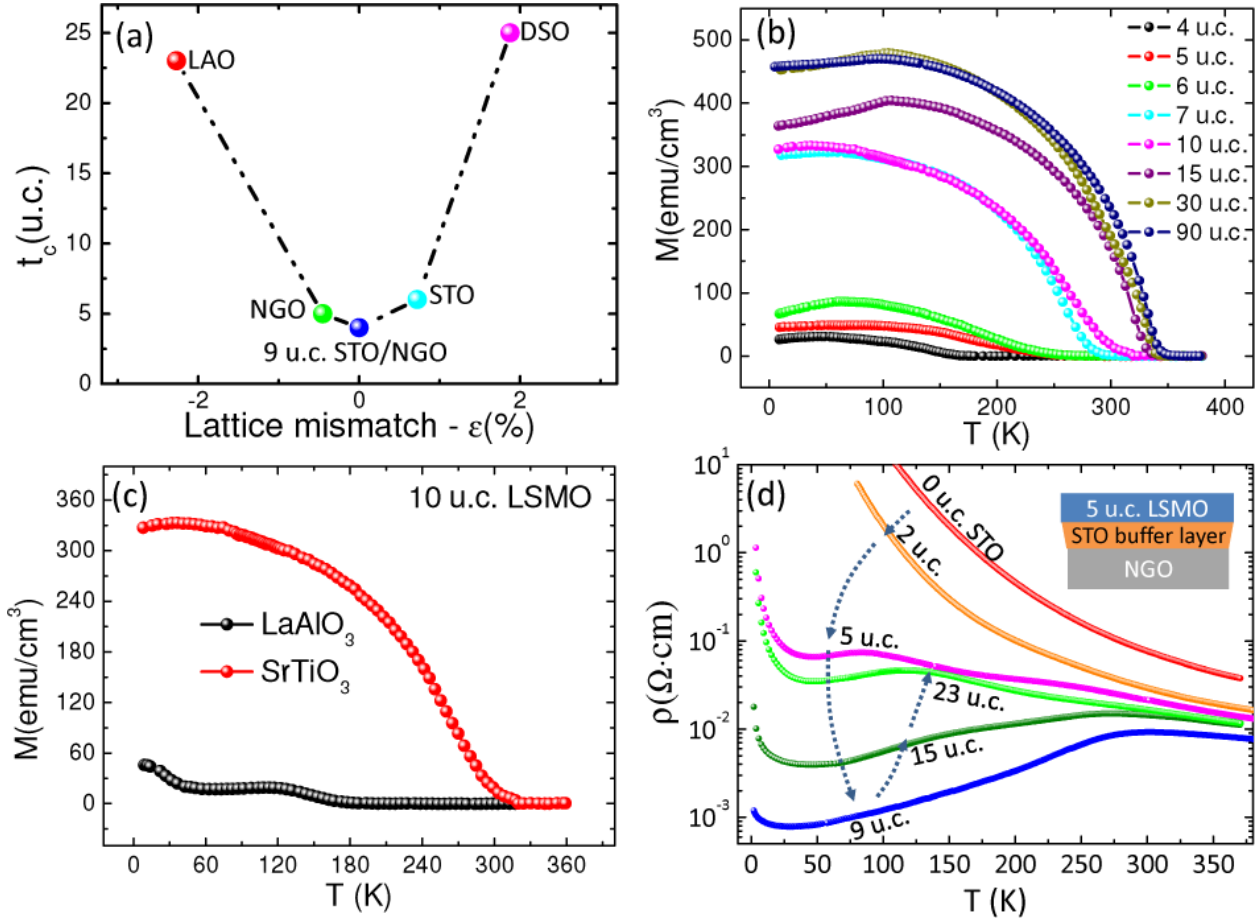


**Figure 3.** (a) Substrate-induced strain dependence of the critical thickness ( $t_c$ ) for MIT in LSMO films. (b)  $T$ -dependent magnetization of different thickness of LSMO films on STO(001). (c)  $T$ -dependent magnetization of 10 u.c. LSMO film on LAO and STO substrates. All samples were field cooled at 1 T from 360 K to 2 K along in-plane [100] before measurement and the magnetization was measured at 150 Oe on warming. (d) Resistivity for a 5 u.c. LSMO film on NGO (110) substrate as a function of STO buffer layer thickness (see the inset for a schematic side view of film arrangement).

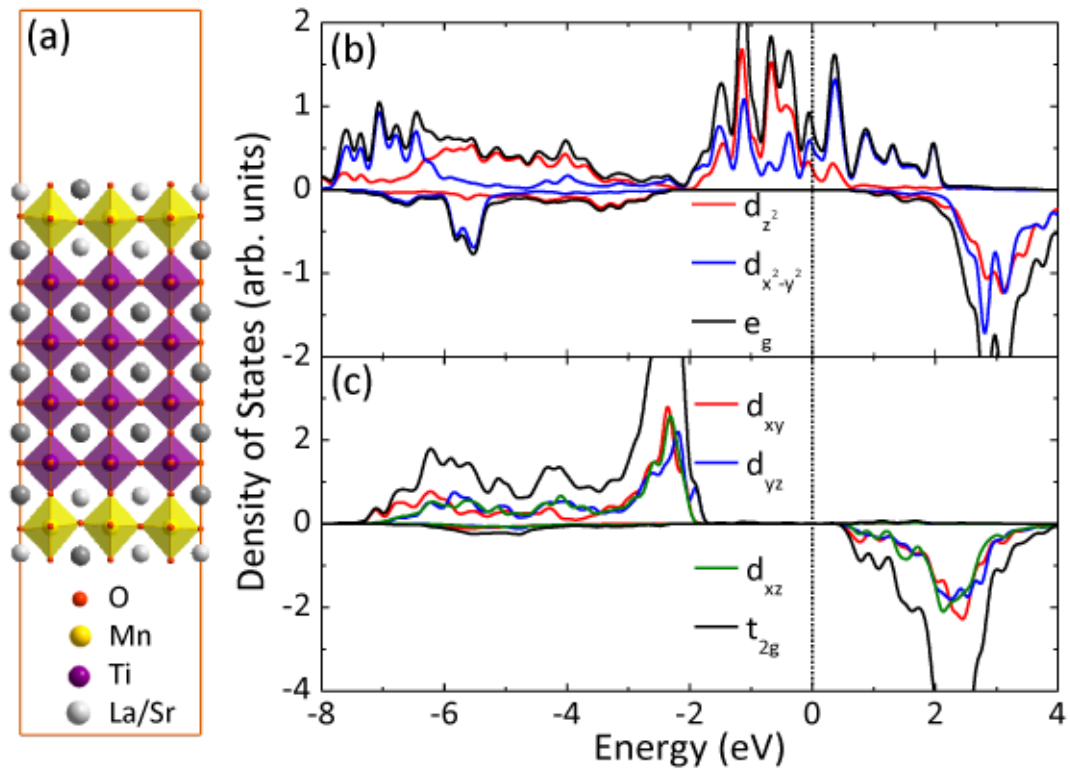


**Figure 4.** (a) The optimized slab model of a single u.c. thickness of LSMO film on STO(001) for the DFT+U ( $U_{\text{Mn}} = 2.0$  eV and  $U_{\text{Ti}} = 8.0$  eV) calculations. The calculated orbital- and spin-resolved densities of states for both (b)  $e_g$  and (c)  $t_{2g}$  orbitals. The single layer LSMO film with ferromagnetic order is subjected to a tensile strain with in-plane lattice constant of  $3.905 \text{ \AA}$ .

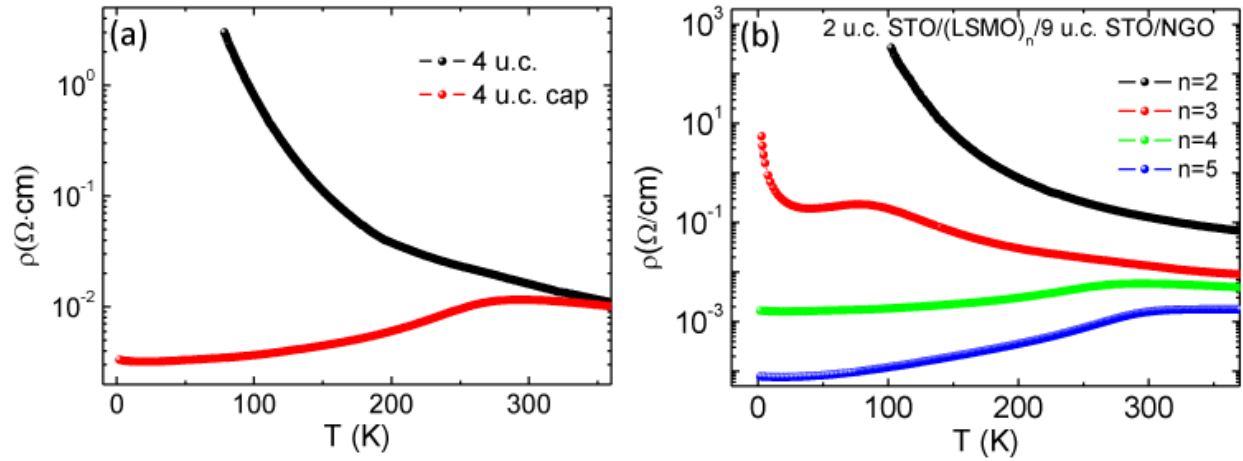


**Fig. 5**  $T$ -dependence of the resistivity for (a) 4 u.c. LSMO grown on a 9 u.c. STO buffered NGO (110) substrate with and without 2 u.c. STO capping; and (b) the different thickness of LSMO films grown on a 9 u.c. STO buffered NGO (110) substrate and capped with 2 u.c. STO capping layer.

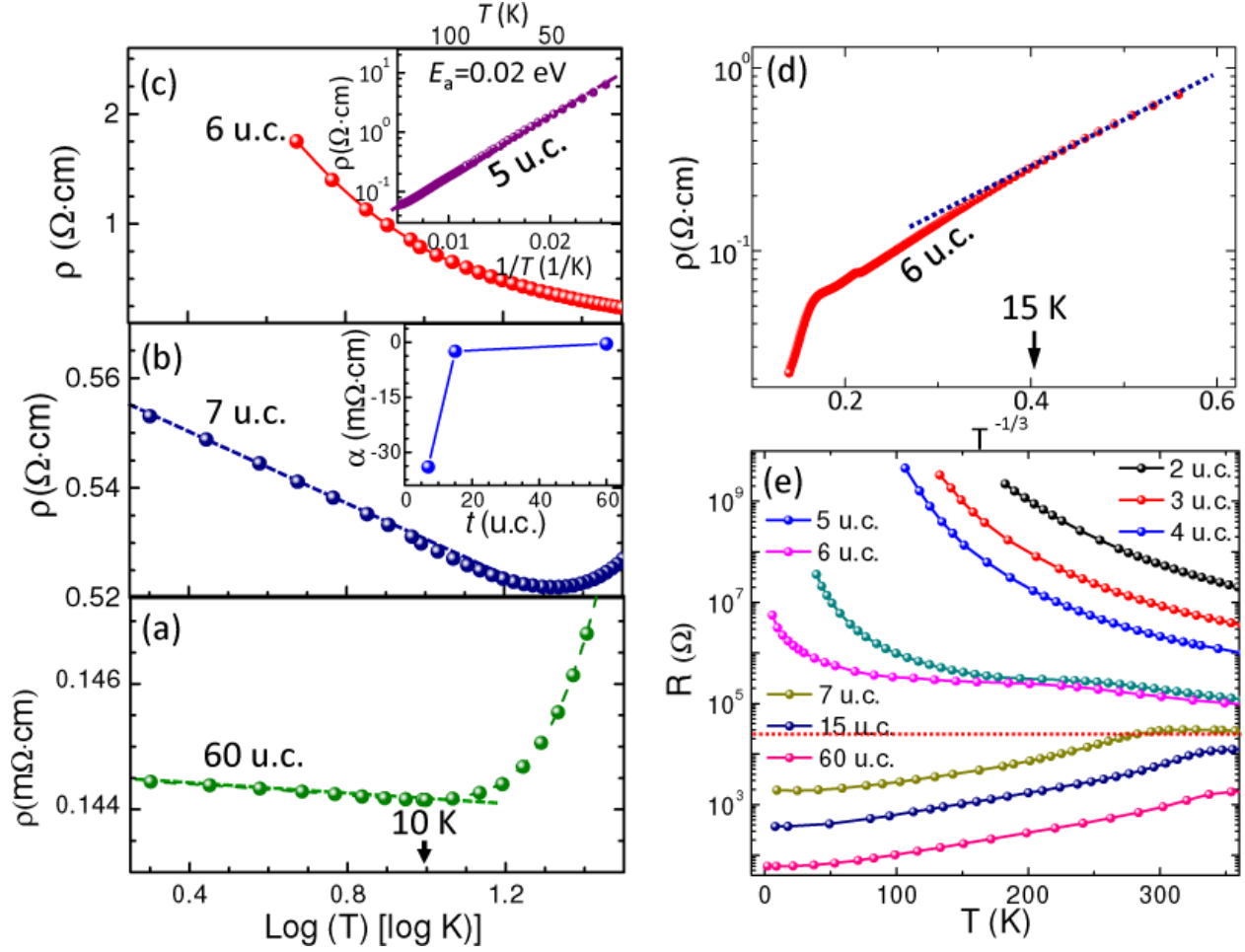


**Figure 6.** The resistivity versus  $\log(T)$  for (a) 60, (b) 7 and (c) 6 u.c. LSMO films on STO (001) in low temperature range. The inset of panel (b) presents the slope ( $\alpha$ ) of resistivity vs.  $\log(T)$  for different film thickness and the inset of panel (c) shows the log-plot of resistivity as a function of  $1/T$  for 5 u.c. film, where the thermal activation energy ( $E_a$ ) is extracted. (d) Log-plot of resistivity as a function of  $1/T^{1/3}$  for 6 uc LSMO/STO(001). (e)  $T$ -dependence of sheet resistance for different thickness of LSMO films grown on STO(001). The red dot line indicates the Ioffe-Regel (IR)-limit for the onset of strong localization. All the films were grown at  $P_O = 130$  mTorr.

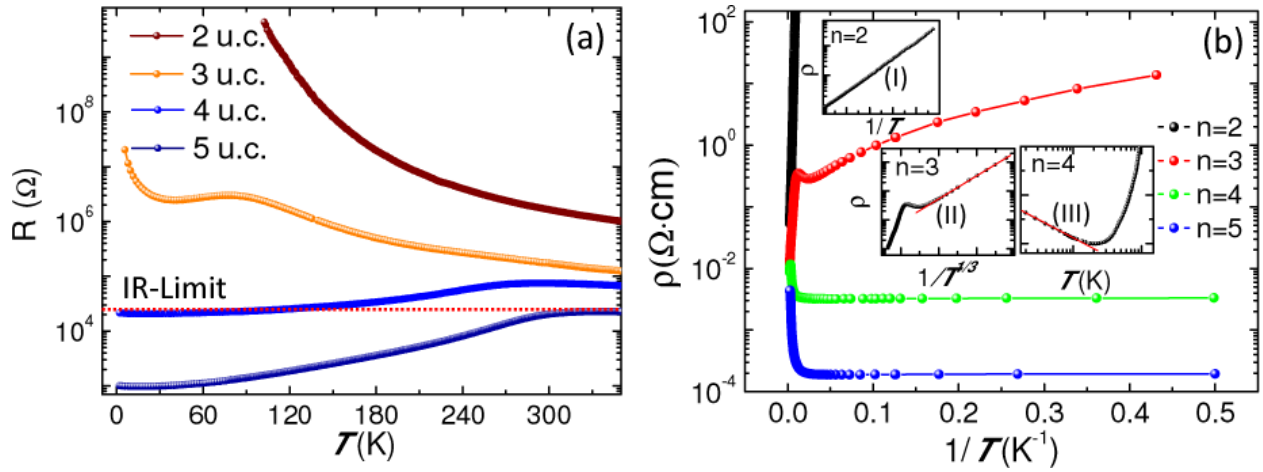


**Figure 7.** (a)  $T$ -dependence of sheet resistance for different thickness of LSMO films grown on 9 u.c. STO buffered NGO with 2 uc STO capping layer at oxygen pressure  $P_{\text{O}} = 130$  mTorr. The red dot line indicates the Ioffe-Regel (IR)-limit for the onset of strong localization. (b) The corresponding Log-plot of resistivity as a function of  $1/T$  respectively. The inset (I) shows the low- $T$  zoom-in plot of (I)  $\log(\rho)$  vs.  $1/T$  for 2 u.c., (II)  $\log(\rho)$  vs.  $1/T^{1/3}$  for 3 u.c., and (III)  $\rho$  vs.  $\log(T)$  for 4 u.c. film, respectively. All the films were grown at  $P_{\text{O}} = 130$  mTorr.